DOI: 10.1002/cplu.201200024

Heterostructured TiO_2 Nanoparticles/Nanotube Arrays: In Situ Formation from Amorphous TiO_2 Nanotube Arrays in Water and Enhanced Photocatalytic Activity

Kaifu Huo,*[a, b] Hairong Wang,[b] Xuming Zhang,[a] Yue Cao,[b] and Paul K. Chu*[a]

Heterostructured TiO_2 nanoparticles/nanotube arrays (NPs/NTAs) are produced from as-anodized amorphous TiO_2 nanotube arrays in water at a temperature as low as 90 °C. The phase and morphology transformation of the as-anodized amorphous TiO_2 nanotube in water can be attributed to a water-induced dissolution and recrystallization mechanism in which the as-anodized amorphous TiO_2 NTAs are gradually self-sacrificed, and then spontaneously morphing into the composite NPs/NTAs structure consisting of anatase NPs and thinner amorphous NTs. The composite can be further crystallized into anatase TiO_2 NPs/NTAs consisting of anatase NT and anatase NPs by annealing in air at 450 °C for 3 hours. The composite anatase TiO_2 NPs/NTAs have a surface area that is 1.4 times larger than that of the anatase TiO_2 NTAs and possess enhanced photocatalytic activity in the photodecomposition of organic pollutants and water splitting. The photodecomposition rate of the organic pollutant rhodamine B by the anatase TiO_2 NPs/NTAs photocatalyst is two times higher than that by the annealed anatase TiO_2 NTAs. The enhanced photocatalytic activity of the hererostructured TiO_2 NPs/NTAs arises from the large surface area of the TiO_2 NPs and superior electron transport in anatase TiO_2 NT. The in situ hydrothermal conversion of the microstructure from amorphous TiO_2 NTAs into hererostructured TiO_2 NPs/NTAs in water is very simple thereby enabling the design and fabrication of highly photoactive one-dimensional TiO_2-based functional materials applicable to photocatalysis and solar energy conversion.

Introduction

Semiconductor photocatalysts have recently received considerable attention owing to their wide applications to environmental purification, solar energy conversion, and water splitting.[1,2] TiO_2 nanoparticles (NPs) such as Degussa P25 have been extensively investigated as a promising photocatalyst to remove environmental pollutants.[3] However, recovery of the suspended TiO_2 NPs from the slurry after the photocatalytic reaction is very difficult and energy consuming. TiO_2 nanotube arrays (TiO_2 NTAs) can overcome such drawbacks and allow easy recovery for recycling usage. Anodization is a relatively simple and efficient method to fabricate highly ordered TiO_2 NTAs on Ti foils or any three-dimensional (3D) nonplanar surfaces.[2,4] The anodized TiO_2 NTAs grow directly and adhere strongly to the underlying Ti substrate, thus allowing easy recovery of the photocatalyst. In addition, the TiO_2 NTAs film possesses improved charge transport properties because the nanotube wall provides a direct path for electron transport resulting in enhanced photoelectrochemical properties.[5] Hence, highly ordered TiO_2 NTAs prepared by electrochemical anodization have attracted increasing attention and are gaining popularity in environmental purification, photoelectrochemical decomposition of water, solar cells, and biological coatings.[6]

The photocatalytic activity and photoelectrochemical properties of TiO_2 are related to its morphology, surface area, phase structure, as well as photogenerated charge separation and transport performance.[7] The as-anodized TiO_2 NTAs are usually in the amorphous state, and so a high-temperature treatment is generally required to form the more photocatalytically active anatase structure. Although the anatase TiO_2 NTAs exhibit high charge transport and collection efficiency, the surface area is smaller than that of nanoparticles or the mesosponge structure, thereby leading to lower dye absorption and light harvesting.[2] In contrast, anatase TiO_2 NPs provide a high surface area for light harvesting, but the random zigzag electron transport paths stifle electron transport in films composed of TiO_2 NPs.[8] In view of these factors, the heterostructured TiO_2 NPs/NTAs composite structure composed of anatase TiO_2 NTAs and anatase NPs should exhibit improved photoelectrochemical properties because they combine the merits of the large surface area of NPs and superior electron transport properties of the NTs. Recently, efforts have been devoted to the fabrication of TiO_2 NPs/NTAs composite nanostructures includ-

[a] Prof. K. Huo, X. Zhang, Prof. P. K. Chu
Department of Physics and Materials Science
City University of Hong Kong
Tat Chee Avenue, Kowloon, Hong Kong (P. R. China)
Fax: (+86) 52-34420542
E-mail: paul.chu@cityu.edu.hk

[b] Prof. K. Huo, H. Wang, Y. Cao
School of Materials and Metallurgy
Wuhan University of Science and Technology
Wuhan 430081 (P. R. China)
Fax: (+86) 27-68862529
E-mail: kfhuo@wust.edu.cn
kaifuhuo@cityu.edu.hk

Supporting information for this article is available on the WWW under http://dx.doi.org/10.1002/cplu.201200024.

ing treating TiO_2 NTAs with $TiCl_4$,[9] filling nanotubes with TiO_2 NPs,[10] putting TiO_2 powder on TiO_2 NTAs surfaces,[11] and electrophoretic deposition of NPs.[12] However, these methods usually need tedious synthesis steps or strict experimental control. In addition, the TiO_2 NPs are easily conglomerated at the mouth of the NTAs and not uniformly distributed along the NT.

Herein, we report a simple and in situ hydrothermal method to controllably fabricate composite TiO_2 NPs/NTAs from as-anodized amorphous TiO_2 NTAs in water at a temperature as low as 90 °C. This hydrothermal process does not require any other additive or Ti precursor except water. Formation of the composite TiO_2 NPs/NTAs from amorphous TiO_2 NTAs is attributed to a water-induced dissolution and recrystallization mechanism[13] in which the as-anodized amorphous TiO_2 NTAs are gradually self-sacrificed, and then spontaneously morphing into the composite NPs/NTAs structure consisting of anatase NPs and thinner amorphous NTs and finally into TiO_2 nanorod arrays (NRAs) composed of connecting anatase NPs. The spontaneously formed composite TiO_2 NPs/NTAs have a surface area 1.4 times larger than that of the annealed anatase TiO_2 NTAs, thus leading to enhanced photocatalytic activity in the photodecomposition of organic pollutants and water splitting in comparison with the pristine TiO_2 NTAs. Moreover, the photocatalytic activity of the hydrothermally formed TiO_2 NPs/NTAs can be further improved by subsequent annealing to form the anatase TiO_2 NPs/NTAs structure. The photodecomposition rate of the organic pollutant rhodamine B (RhB) on the anatase TiO_2 NPs/NTAs photocatalyst is two times larger than that on the annealed anatase TiO_2 NTAs. The in situ hydrothermal conversion of the microstructure from amorphous TiO_2 NTAs to NPs/NTAs in water is very simple and environmentally friendly. Furthermore, if a metal (M) ion is present in water, the heterostructured $MTiO_3$ NPs/TiO_2 NTAs can be easily obtained by a similar hydrothermal treatment of amorphous TiO_2 NTAs. The results presented herein are applicable to the design and fabrication of highly photoactive 1D TiO_2-based functional materials, which have potential use in photocatalysis and solar energy conversion.

Results and Discussion

Figure 1a depicts the typical top-view image of the field-emission scanning electron microscopy (FE-SEM) image of the NTAs fabricated by anodization in an ethylene glycol electrolyte containing 0.5 wt% NH_4F and 5 vol% distilled (DI) water at 60 V for 1 hour, showing that uniform NTAs with an inner diameter of 110 nm and wall thickness of 15 nm are formed. The side view FE-SEM image in Figure 1b reveals that the NT has a smooth outside surface and the length of NTAs is about 6 μm. Although the outer diameter remains the same, the wall thickness of the NT increases with depth from 15 nm at the top to 50 nm on the bottom. The transmission electron microscopy (TEM) image in Figure 1c also shows the gradually thickened wall with depth. The diffuse ring of selected-area electron diffraction (SAED) pattern in the inset of Figure 1c of the single NT indicates the amorphous nature of the as-anodized NTAs. The glancing angle XRD pattern (GAXRD, glancing angle

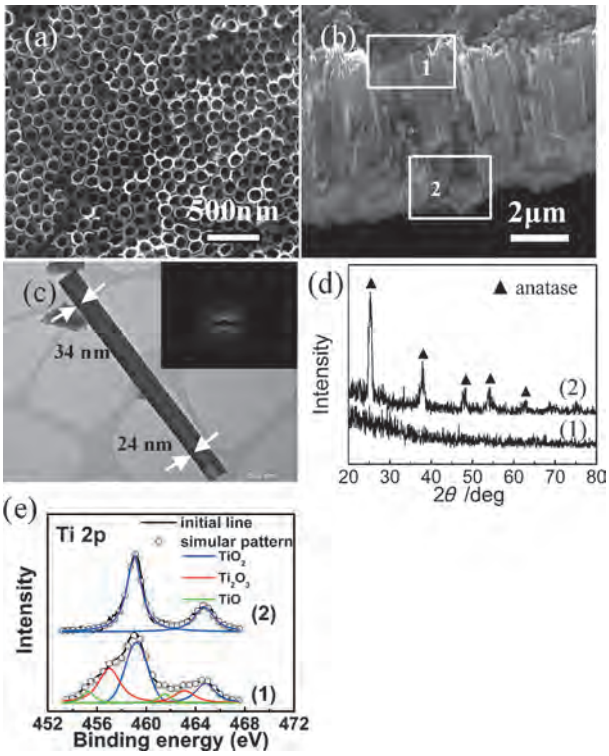

Figure 1. a) Top-view and (b) side-view of FE-SEM images of the as-anodized TiO_2 NTAs, suggesting that uniform NTAs are formed on the Ti foil. The wall thickness of NT increases with depth from 15 nm on top (rectangle 1 in (b)) to 50 nm on the bottom (rectangle 2 in (b)). c) TEM images of a single NT and corresponding SAED pattern (inset). d) and e) XRD pattern and fine XPS spectra of Ti(2p) of as-anodized TiO_2 NTAs (curve 1) and annealed TiO_2 NTAs at 450 °C for 3 h in air (curve 2).

of 1°) of the as-anodized NTAs shows no diffraction peaks of any TiO_2 phases, thus further indicating the amorphous nature of the as-anodized NTAs (curve 1 in Figure 1d). However, the anatase TiO_2 peaks can be clearly observed when the as-anodized NTAs are annealed at 450 °C for 3 hours in air (curve 2 in Figure 1d). The high-resolution X-ray photoelectron spectroscopy (XPS) Ti(2p) spectra of the as-anodized NTAs after Ar sputtering for 10 nm are located at 455.3/461.5 eV, 457/463.1 eV, and 464.8/459.3 eV (curve 1 in Figure 1e) corresponding to Ti^{2+}/TiO, Ti^{3+}/Ti_2O_3, and Ti^{4+} in TiO_2, respectively, thus suggesting that the as-anodized NTAs contain a large amount of suboxide species.[14] However, when the NTAs are annealed at 450 °C for 3 hours in air, only the Ti(2p) peaks corresponding to Ti^{4+} in TiO_2 exist (Figure 1e, Curve 2). The results evidently suggest that the anodized titania NTAs are amorphous and composed of not only TiO_2 but also an abundant amount of titanium suboxide species such as TiO and Ti_2O_3.

The as-anodized amorphous TiO_2 NTAs on Ti are not stable in water under hydrothermal conditions. They are first converted into the composite TiO_2 NPs/NTAs structure and finally mesoporous anatase TiO_2 NRAs. Figure 2a–c depicts the SEM images of the as-anodized amorphous TiO_2 NTAs after hydrothermal treatment in water at 90 °C for different periods of time (3–4 h). Image a in Figure 2 depicts the FE-SEM image of the pristine as-anodized TiO_2 NTs hydrothermally treated in

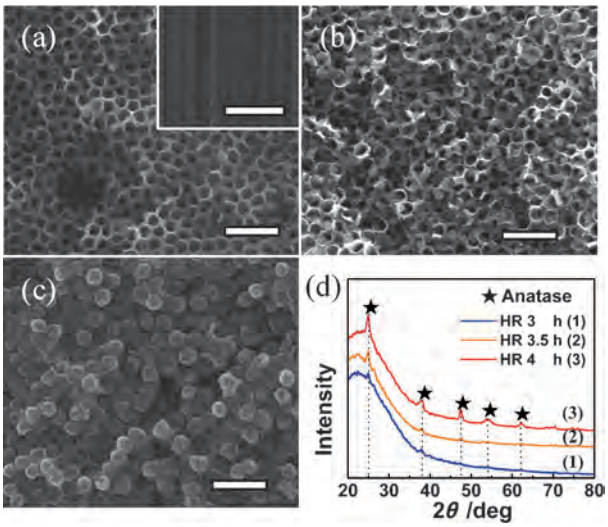

Figure 2. FE-SEM images of amorphous TiO_2 NTAs formed by hydrothermal reaction (HR) in water at 90 °C for (a) 3 h, (b) 3.5 h, and (c) 4 h. d) Corresponding XRD patterns of the three sample in (a)–(c). The scale bar is 500 nm.

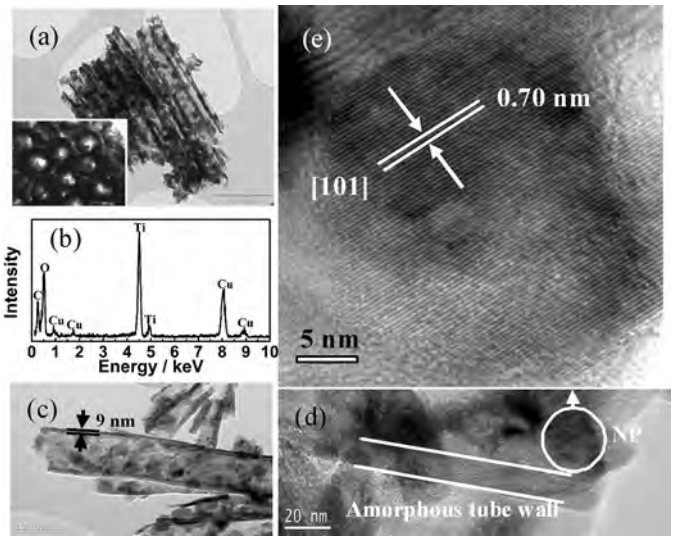

Figure 3. a) Typical TEM image of composite structure of TiO_2 NPs/NTAs shown in Figure 2b. b) Corresponding EDS spectrum. c–e) HR-TEM micrographs of the composite structure of TiO_2 NPs/NTAs.

water for over 3 hours at 90 °C, and indicates that many small particles with a size of 10 nm are formed and uniformly attached on the surface of NT to form the composite NPs/NTAs structure. When the hydrothermal treatment time is increased to 3.5 hours, more and bigger particles with a size of 20–30 nm are formed. At the same time, the nanotube wall becomes thinner although the tubular structure is retained. After increasing the hydrothermal treatment time to over 4 hours, the original morphology of NTAs is not visible, but instead NRAs are formed (Figure 2c). The XRD patterns obtained at different hydrothermal treatment time are depicted in Figure 2d. The anatase TiO_2 diffraction peaks can be clearly observed from the samples after 3 hours of hydrothermal reaction and the relative intensity of the anatase TiO_2 peaks increases when the NTAs are fully converted into NRAs.

Figure 3 displays the representative TEM micrographs and energy-dispersive X-ray spectroscopy spectrum of the composite TiO_2 NPs/NTAs corresponding to the sample shown in Figure 2b. Figure 3a indicates that NPs with a size 20–30 nm are attached onto the inner wall of the NT forming the composite NPs/NT structure. The EDS spectrum of the composite (Figure 3b) reveals well-resolved and strong signals of Ti and O, thus suggesting that the NPs/NT composites are composed of mainly Ti and O. In comparison with the pristine as-anodized NT with a tube wall thickness of 15 nm, the thickness of the tube wall in the composite NPs/NT is thinner and about 9 nm as shown in Figure 3c. Because there is no extraneous Ti source, the NPs should be from the NT wall, which is formed by partial self-sacrifice and recrystallization. The high-resolution TEM (HR-TEM) images in Figure 3d,e suggests that the NPs comprise crystallized anatase phase, but the NT wall still remains in the amorphous state. The distance of 0.35 nm between two neighboring fringes of the NP can be clearly identified in Figure 3e. It corresponds to the d-spacing of [101] planes of anatase TiO_2. The results evidently demonstrate that the heterostructured nanostructures composed of anatase NPs and amorphous NTs can be spontaneously and controllably synthesized in situ by using a mild hydrothermal reaction at 90 °C without any foreign reactants except water. This heterostructure composed of anatase TiO_2 NPs and amorphous NT can be further converted into anatase TiO_2 NPs/NTAs consisting of anatase NPs and anatse NT by annealing at 450 °C for 3 hours in air.

The microstructure and morphology of the NRAs are also investigated. Figure 4a shows the typical FE-SEM images of the NRAs and the NRAs have similar geometrical dimensions (130 nm in diameter and 6 μm in length) in comparison with the pristine amorphous NTAs. The representative TEM image of a single NR suggests that the NR is composed of accumulated NPs as shown in Figure 4b. The NPs have a diameter of 30–50 nm and are linked together to form a NR. The HR-TEM picture in Figure 4c reveals single-crystalline anatase TiO_2 and it is consistent with the XRD data in Figure 2d.

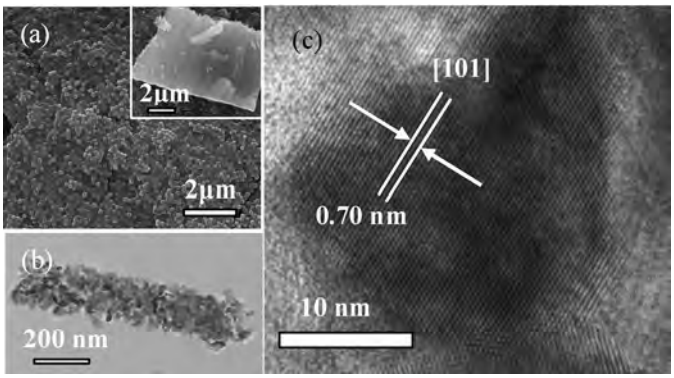

Figure 4. a) Top-view of FE-SEM image of nanorod arrays. The inset is the cross-sectional image of a typical TEM image of (b) single NR composed of incompactly accumulated NPs. c) Lattice-resolution HR-TEM image of the NR.

The hydrothermal temperature affects the transformation rates of amorphous TiO_2 NTAs to NPs/NTAs and finally anatase TiO_2 NRAs in water. At a higher temperature such as 200 °C, amorphous TiO_2 NTAs can only retain its pristine morphology within 35 minutes (Figure S1a in the Supporting Information). After 40 minutes, the smooth surface of NTAs becomes rough and particles emerge on the surface (Figure S1b). When the hydrothermal reaction time is increased to 45 minutes, the pristine morphology of NTAs disappears completely and NRAs are formed (Figure S1d). However, at a lower temperature of 80 °C, the amorphous TiO_2 NTAs can retain the original tubular morphology after undergoing the hydrothermal reaction over 8 hours (Figure S2c).

To explore the role of water in the spontaneous phase and morphological transformation from amorphous TiO_2 NTAs to NPs/NTAs and NRAs, the as-anodized amorphous TiO_2 NTAs are also hydrothermally treated in pure ethanol and a mixture of ethanol and water under the same experimental conditions. In 40 mL of pure ethanol (Figure 5a), the amorphous TiO_2 NTAs retain the original ordered tubular structure at 200 °C for 6 hours. However, by adding 1 mL water to 40 mL of ethanol (Figure 5b), some NPs appear and composite NPs/NTAs are produced. When the amount of water is increased to 2 mL, the quantity of NPs increase and the size becomes bigger as shown in Figure 5c. After adding 4 mL of water, the nanotubular structure vanishes completely and TiO_2 NRAs are formed instead (Figure 5d). The corresponding XRD patterns of the sample obtained with different water amounts are depicted in Figure 5e. No diffraction peaks related to anatase phase can be observed from the sample hydrothermally treated in pure ethanol. However, the strong anatase peaks can be observed clearly from samples hydrothermally treated in the ethanol and water mixture. In addition, the relative intensity of the anatase peaks is enhanced with larger water contents.

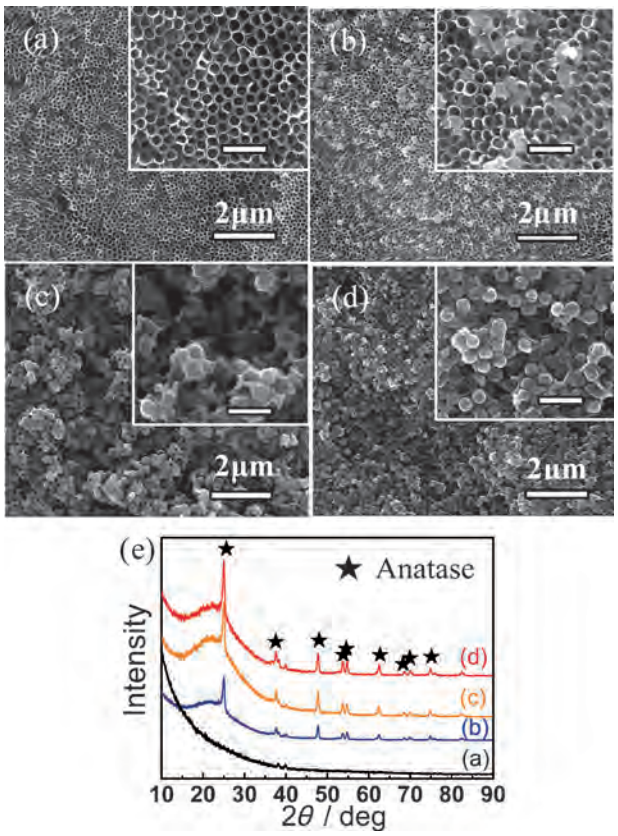

Figure 5. SEM images of as-anodized amorphous TiO_2 NTAs after hydrothermal treatment at 200 °C for 6 h in 40 mL ethanol containing various concentration water, (a) 0 mL, (b) 1 mL, (c) 2 mL, and (d) 4 mL. e) Corresponding XRD patterns without annealing. The scale bar in inset is 500 nm.

Our results indicate that the morphology and phase evolution from amorphous titania to NPs/NTAs and finally NRAs under hydrothermal conditions are governed by water-assisted dissolution and precipitation. As schematically shown in Figure 6, when the amorphous titania NTAs are hydrothermally

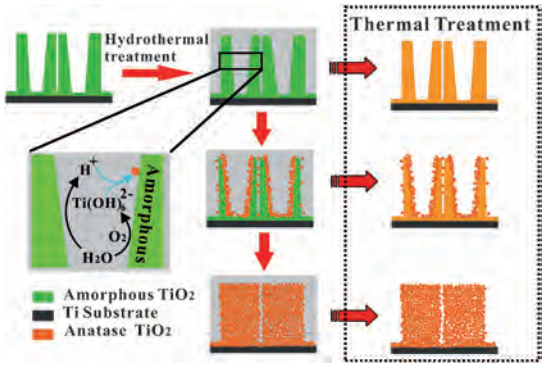

Figure 6. Schematic diagram of water molecule induced phase and morphological evolution of the amorphous NTs under hydrothermal conditions.

treated in water, the unstable TiO_6^{2-} octahedrons of amorphous TiO_2 and titanium suboxide species first absorb water molecules through the surface hydroxy groups to form insoluble species of $Ti(OH)_6^{2-}$, which can be further dehydrated and precipitated by bridging together and sharing faces to form anatase TiO_2. The overall reaction is described as follows by Equations (1) and (2):

$$TiO_x + 4H_2O + (1\text{-}x/2)O_2 \rightarrow Ti(OH)_6^{2-} + 2H^+ \ (1 < x \leq 2) \quad (1)$$

$$Ti(OH)_6^{2-} + 2H^+ \rightarrow TiO_2 + H_2O \quad (2)$$

The freshly formed TiO_2 NPs attach onto the surface of the remaining amorphous TiO_2 NT wall and consequently, heterostructured TiO_2 NPs/NTAs composed of anatase NPs and amorphous NT are produced as schematically shown in Figure 6. In this process, the NPs are only from the self-sacrificed amorphous NT wall because there is no foreign Ti source. As a result, the nanotube thickness of the NPs/NTAs becomes thinner compared to the pristine amporphous NTAs as shown in Figure 1c and Figure 3c. Because the space between the adjacent TiO_2 NTs of a few nanometers is far smaller than the interior of the NTs of about 100–110 nm, water molecules can easily access the inner surface and dissolution/precipitation of TiO_2 onto the inner shell of the tube walls is more kinetically favorable. Therefore, anatase TiO_2 NPs are formed and attach onto the inner surface of the remaining TiO_2 NT, thus resulting

in the formation of composite NPs/NTAs composed of anatase TiO_2 NPs and amorphous TiO_2 NT, as schematically illustrated in Figure 6.

The remaining amorphous nanotube wall of the composite NPs/NTAs can be further etched by water molecules until the tube wall disappears under hydrothermal conditions, and thus the mesoporous anatase TiO_2 NRAs are finally formed as schematically shown in Figure 6. Owing to the presence of titanium suboxide species in the NT wall, oxygen molecules dissolved in water participate in the in situ hydrothermal conversion of the microstructure from amorphous TiO_2 NTAs to hererostructured TiO_2 NPs/NTAs as suggested by Equation (1). If the dissolved oxygen in water is eliminated by purging with high purity N_2 for 1 hour and the Teflon-lined autoclave was sealed while the hydrothermal reaction was carried out under similar experimental conditions, then the NTs still retain the tubular morphology after hydrothermal treatment as shown by Figure S3.

The hydrothermally and spontaneously formed composite NPs/NTAs could crystallize into anatase TiO_2 NPs/NTAs by thermal annealing at 450 °C for 3 hours in air. The anatase TiO_2 NPs/NTAs have good hydrothermal stability and could retain the NPs/NTAs composite structure under hydrothermal conditions (Figure S4). The surface areas of the TiO_2 NTAs, TiO_2 NPs/NTAs composite, and mesoporous anatase TiO_2 NRAs are measured to be 36.2, 49.0, and 52.4 m^2g^{-1} according to Brunauer–Emmett–Teller (BET) analysis through N_2 adsorption (Figure S5). The results provide evidence that anatase NPs/NTAs composite and mesoporous anatase TiO_2 NRAs with a larger surface area can be easily and controllably fabricated from as-anodized amorphous TiO_2 NTAs by a water-induced dissolution and recrystallization process.

The photocatalytic activity of the TiO_2 NTAs, composite TiO_2 NPs/NTAs (hydrothermal reaction (HR) for 3 h), and mesoporous TiO_2 NRAs is evaluated by means of photodegradation of rhodamine B (RhB) in an aqueous solution under illumination with UV light and compared to that of the thermally annealed counterparts treated at 450 °C in air for 3 hours. The results are depicted in Figure 7a. The as-anodized amorphous TiO_2 NTAs exhibit weak photocatalytic activity owing to the amorphous nature, but on the other hand, the hydrothermally formed TiO_2 NPs/NTAs and mesoporous TiO_2 NRAs show obviously enhanced photocatalytic activity. When the three samples are annealed at 450 °C for 3 hours in air, the mesoporous TiO_2 NRAs show no discernible change in the photocatalytic activity because the hydrothermally obtained mesoporous NRAs already have an anatase structure and heat treatment cannot alter the phase and crystalline structure. However, the annealed TiO_2 NTAs and TiO_2 NPs/NTAs exhibit clearly improved photocatalytic activity relative to their counterparts without calcination because thermal calcination in air at 450 °C enables the amorphous nanotube walls to crystallize into the more photocatalytically active anatase structure. In comparison with anatase TiO_2 NTAs, the as-obtained mesoporous TiO_2 NRAs show improved photocatalytic activity owing to the improved surface area and the annealed anatase TiO_2 NPs/NTAs has the highest photocatalytic activity among the samples. The excellent photocatalytic property of heterostructured anatase

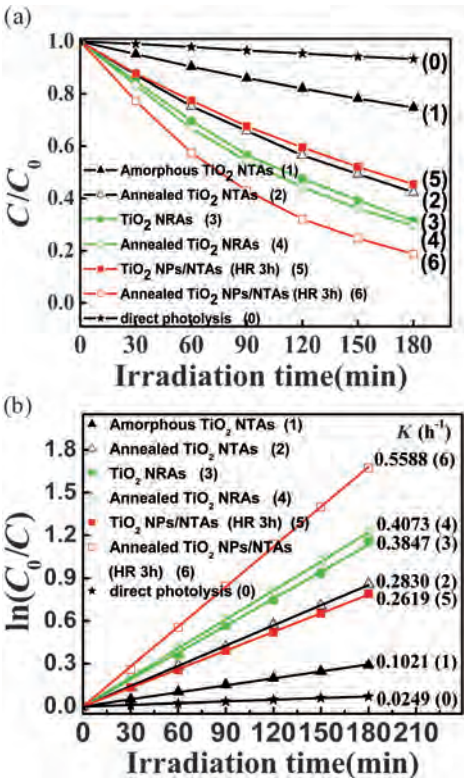

Figure 7. a) Concentration (C) changes of RhB in aqueous solution as a function of illumining time (t) under UV light irradiation in the presence of photocatalyst of TiO_2 NTAs, TiO_2 NPs/NTAs, and mesoporous TiO_2 NRAs. The photodegradation reaction follows the first-order reaction kinetics and the apparent rate constants (k) are listed in b).

TiO_2 NPs/NTAs can be attributed to the combined merits of the large surface area of the TiO_2 NPs and superior electron transport properties of anatase TiO_2 NT. The photodegradation behavior of RhB in the presence of these photocatalysts obey the first-order reaction kinetics expressed as $\ln(C_0/C) = kt$, where k is the rate constant, t is the irradiation time, and C_0 and C are the initial and reaction concentrations of the RhB aqueous solution, respectively. As shown in Figure 7b. The k value of as-thermal mesoporous NRAs is 0.4 h^{-1} and 1.5 times larger than that of anatase TiO_2 NTAs. The enhancement in photocatalytic activity of the mesoporous TiO_2 NRAs can be ascribed to the larger surface area according to the BET analysis shown in Figure S5. The annealed TiO_2 NPs/NTAs possess the highest photocatalytic activity among the samples and the k value of the annealed TiO_2 NPs/NTAs is 0.56 h^{-1}, which is two times larger than that of the annealed TiO_2 NTAs. However, the photocatalytic activity cannot be fully accounted for by the improved surface area, because the surface area of the anatase TiO_2 NPs/NTAs is merely 1.4 times larger than that of the thermally annealed TiO_2 NTAs. In addition, the mesoporous TiO_2 NRAs have a larger surface area than the anatase TiO_2 NPs/NTAs, but inversely, the annealed TiO_2 NPs/NTAs have higher photocatalytic activity than the mesoporous TiO_2 NRs.

Figure 8a,b displays the photocurrent density as a function of applied potential (vs. Ag/AgCl) and transient photocurrent responses in a 0.5 M Na_2SO_4 solution under UV irradiation of

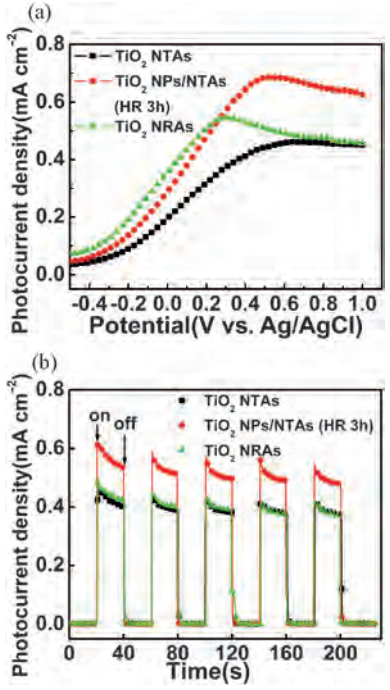

Figure 8. Photocurrent density as a function of applied potential (vs. Ag/AgCl; a) and transient photocurrent responses (b) in a 0.5 M Na_2SO_4 solution under UV irradiation for the samples of annealed TiO_2 NTAs, TiO_2 NPs/NTAs, and TiO_2 NRAs electrodes.

the annealed TiO_2 NTAs, TiO_2 NPs/NTAs, and TiO_2 NRAs electrodes. The average photon intensity reaching the sample surface is measured to be about 5.0 mW cm^{-2} and the anodic bias potential is scanned from -0.5 to $+1$ V at a rate of 10 mV s^{-1}. Figure 8a shows the photocurrent of these structures under UV irradiation. The dark current (DC) without UV irradiation is almost zero and negligible, but the PC measured from the three samples increase dramatically with anodic potential. The saturated photocurrent for TiO_2 NTAs and mesoporous TiO_2 NRAs are about 0.46 and 0.52 mA cm^{-2} at an applied potential of 0.5 V (vs. Ag/AgCl). However, the PC measured from the composite TiO_2 NPs/NTAs at a bias of 0.5 V is 0.68 mA cm^{-2}, which is 1.5 and 1.2 times larger than those of the TiO_2 NTAs and mesoporous TiO_2 NRAs, respectively. Although the mesoporous TiO_2 NRAs have the largest surface area, the random zigzag electron paths through the connected NPs structure result in high recombination and depletion of the photoexcited electrons and holes, thus lowering the photoelectrochemical efficiency. We further examine the photocurrent response of the three samples with time and the amperometric *I–t* curves collected with light on/off cycles at 0.5 V bias (vs. Ag/AgCl) are shown in Figure 8b. The TiO_2 NRAs have poor transient photocurrents but those of TiO_2 NPs/NTAs during illumination are about 1.32 times larger than that of annealed TiO_2 NTAs. The photocatalytic and photoelectrochemical results strongly suggest that the TiO_2 NPs/NTAs formed by the in situ hydrothermal treatment and subsequent calcination are promising photocatalysts for environmental purification, photoelectrochemical water decomposition, and solar cell applications.

Conclusion

Heterostructured TiO_2 nanoparticles/nanotube arrays (NP/NTAs) are produced spontaneously from as-anodized amorphous TiO_2 nanotube arrays in water at a temperature as low as 90 °C. The phase and morphological transformation of the as-anodized amorphous TiO_2 nanotubes in water are characterized and a mechanism encompassing water induced dissolution and recrystallization is proposed. The amorphous TiO_2 nanotube wall can be gradually etched by water molecules and converted into anatase nanoparticles, which are attached onto the remaining thinner amorphous nanotube wall, thus resulting in the formation of the composite NPs/NTAs structure. The TiO_2 NPs/NTAs have an improved surface area that is about 1.4 times larger than that of the pristine TiO_2 NTAs. The photocatalytic activity can be further improved by annealing to form the anatase TiO_2 NPs/NTAs structure composed of anatase NPs and NT by annealing in air at 450 °C for 3 hours. The photodecomposition rate of the organic pollutant RhB on the anatase TiO_2 NPs/NTAs photocatalyst is two times larger than that on the annealed anatase TiO_2 NTAs. The enhanced photocatalytic activity achieved from the hererostructured TiO_2 NPs/NTAs is ascribed to the large surface area of TiO_2 NPs and superior electron transport in the anatase TiO_2 NT. The results suggest a facile and practical route to improve the photocatalytic activity of composite NPs/NTAs by simple hydrothermal modification and also pave the way for the design of various TiO_2-related functional materials by doping, deposition, and sensitization applicable to photocatalysis and solar energy conversion.

Experimental Section

Fabrication of amorphous titanium oxide nanotube arrays and in situ hydrothermal transformation into composite anatase TiO_2 nanoparticles/nanotube arrays

The amorphous titanium oxide nanotube arrays were fabricated by electrochemical anodization. In brief, Ti foils (99.7% pure, Aldrich, $10\times20\times1$ mm^3) were first polished by SiC sandpaper and then ultrasonically cleaned with acetone, ethanol, and deionized water sequentially. Electrochemical anodization was carried out in a two electrode configuration with a graphite plate cathode and Ti foil anode. After anodization in an ethylene glycol solution with 0.5 wt% NH_4F and 5 vol% H_2O at 60 V for 1 hour, the samples were rinsed in distilled (DI) water and dried in air. Then the samples were annealed at 200 °C in air to strengthen adhesion between the Ti substrate and as-anodized NTAs film. Afterwards, the samples were placed vertically and immerged in 40 mL of H_2O solution in a 60 mL Teflon-lined autoclave on a holder. The autoclave was sealed and heated in an oven for different time periods. After the hydrothermal reaction, the specimens were removed from the vessel and ultrasonically washed with DI water for 5 minutes and then dried in air to obtain the sample of composite anatase TiO_2 nanoparticles/nanotube arrays (TiO_2 NPs/NTAs).

Characterization methods

The samples were characterized by glancing angle X-ray diffraction with $Cu_{K\alpha}$ radiation ($\lambda = 1.5418$ Å; XRD, Philips X'Pert Pro), field-

emission scanning electron microscopy, (FE-SEM, FEI Nova 400 Nano), energy dispersive X-ray spectroscopy (EDS, Oxford INCA 200), transmission electron microscopy (TEM; Philips CM20), high-resolution TEM (HR-TEM; JEM-2010F), as well as X-ray photoelectron spectroscopy (XPS, ESCALB MK-II). The N_2 adsorption/desorption measurements were carried out at $-196\,^{\circ}C$ after drying in vacuum at $100\,^{\circ}C$ for 6 hours on a CHEMBET-3000, and the BET (Brunauer–Emmett–Teller) surface areas of the samples were calculated using the BET equation.

Photocatalysis and photoelectrochemical measurement

The photocatalytic activity was assessed by photodegradation of RhB in an aqueous solution. The sample with a size of $1\times1\,cm^2$ was immersed in an aqueous solution of RhB (20 mL) with an initial concentration of $2.5\,mg\,L^{-1}$. The solution was stirred in darkness for 2 hours to saturate the photocatalyst with RhB. The photodegradation experiments were performed at the natural pH of the RhB dye. The solution was aspirated continuously with air during the photocatalytic reaction. A high pressure mercury lamp (500 W, primary wavelength of 365 nm) was used as the UV irradiation source and the average UV intensity impacting the samples surface was measured to be $5.0\,mW\,cm^{-2}$ using irradiance meters (Model: UV-A, Beijing Normal University, China). The change in the RhB concentration with photocatalytic time was measured using a UV/Vis spectrophotometer (TU-1810SPC, Beijing PGENERAL, Beijing, China).

The photoelectrochemical characteristics of the anatase TiO_2 NTAs, TiO_2 NPs/NTAs, and TiO_2 NRAs were evaluated using a three electrode photoelectrochemical cell under the same Hg lamp. The samples were insulated with epoxy resin leaving an open area of $1\times1\,cm^2$ as the working photoanode. An Ag/AgCl electrode served as the reference electrode and a platinum foil was the counter electrode. All the photocurrent experiments were performed on a CHI650c potentiostat (CH Instruments Inc. Shanghai, China). The current–voltage (*I–V*) characteristics were measured by linear sweep voltammetry at a scanning rate of $10\,mV\,s^{-1}$ in a 0.5 M Na_2SO_4 solution. The current–time curves (*I–t*) were obtained with a 0.5 V bias using the same incident light source.

Acknowledgements

This study was supported by the National Natural Science Foundation of China (50902104) and the Hong Kong Research Grants Council (RGC) General Research Funds No CityU 112510.

Keywords: hydrothermal reaction · nanocomposites · photocatalytic activity · photoelectrochemistry · TiO_2

[1] a) A. Fujishima, K. Honda, *Nature* **1972**, *238*, 37–38; b) N. Vlachopoulos, P. Liska, J. Augustynski, M. Graetzel, *J. Am. Chem. Soc.* **1988**, *110*, 1216–1220; c) B. O'Regan, M. Gratzel, *Nature* **1991**, *353*, 737–740; K. Macounová, H. Krsova, J. Ludvmk, J. Jirkovsk, *J. Photochem. Photobiol. A* **2003**, *156*, 273–282; d) Z. Zheng, B. Huang, X. Qin, X. Zhang, Y. Dai, *Chem. Eur. J.* **2010**, *16*, 11266–11270.

[2] K. Lee, D. Kim, P. Roy, I. Paramasivam, B. I. Birajdar, E. Spiecker, P. Schmuki, *J. Am. Chem. Soc.* **2010**, *132*, 1478–1479.

[3] a) J. Grzechulska, A. W. Morawski, *Appl. Catal. B* **2003**, *46*, 415–419; b) T. Ohno, K. Sarukawa, K. Tokieda, M. Matsumura, *J. Catal.* **2001**, *203*, 82–86.

[4] a) D. W. Gong, C. A. Grimes, O. K. Varghese, W. C. Hu, R. S. Singh, Z. Chen, E. C. Dickey, *J. Mater. Res.* **2001**, *16*, 3331–3334; b) M. Paulose, H. E. Prakasam, O. K. Varghese, L. Peng, K. C. Popat, G. K. Mor, T. A. Desai, C. A. Grimes, *J. Phys. Chem. C* **2007**, *111*, 14992–14997; c) Y. Liu, H. Wang, J. M. Xu, Q. H. Ye, H. Shen, *J. Phys. D* **2010**, *43*, 205103–205109.

[5] a) P. E. de Jongh, D. Vanmaekelbergh, *Phys. Rev. Lett.* **1996**, *77*, 3427–3430; b) A. Wolcott, W. A. Smith, T. R. Kuykendall, Y. Zhao, J. Z. Zhang, *Small* **2009**, *5*, 104–111; c) H. F. Zhuang, C.-J. Lin, Y.-K. Lai, L. Sun, J. Li, *Environ. Sci. Technol.* **2007**, *41*, 4735–4740.

[6] a) C. A. Grimes, G. K. Mor in *TiO_2 Nanotube Arrays: Synthesis Properties, and Applications*, Springer, New York, **2009**; b) X. Pan, C. H. Chen, K. Zhu, Z. Y. Fan, *Nanotechnology* **2011**, *22*, 235402; c) X. Xu, X. Fang, T. Zhai, H. Zeng, B. Liu, X. Hu, Y. Bando, D. Golberg, *Small* **2011**, *7*, 445–449.

[7] a) M. Grätzel, *J. Photochem. Photobiol. A* **2004**, *164*, 3–14; b) M. Paulose, G. K. Mor, O. K. Varghese, K. Shankar, C. A. Grimes, *J. Photochem. Photobiol. A* **2006**, *178*, 8–15; c) G. K. Mor, O. K. Varghese, M. Paulose, K. Shankar, C. A. Grimes, *Sol. Energy Mater. Sol. Cells* **2006**, *90*, 2011–2075.

[8] D. Kim, A. Ghicov, S. P. Albu, P. Schmuki, *J. Am. Chem. Soc.* **2008**, *130*, 16454–16455.

[9] a) P. M. Sommeling, B. C. O'Regan, R. R. Haswell, H. J. P. Smit, N. J. Bakker, J. J. T. Smits, J. M. Kroon, J. A. M. van Roosmalen, *J. Phys. Chem. B* **2006**, *110*, 19191–19197; b) F. J. Knorr, D. Zhang, J. L. McHale, *Langmuir* **2007**, *23*, 8686–8690; c) P. Roy, D. Kim, I. Paramasivam, P. Schmuki, *Electrochem. Commun.* **2009**, *11*, 1001–1004.

[10] Y. H. Chen, K.-C. Huang, J. G. Chen, R. Vittal, K. C. Ho, *Electrochim. Acta* **2011**, *56*, 7999–8004.

[11] Y. Alivov, *Appl. Phys. Lett.* **2009**, *95*, 063504.

[12] K. Shin, Y. Jun, G. Y. Han, J. H. Park, *J. Nanosci. Nanotechnol.* **2009**, *9*, 7436–7439.

[13] a) D. Wang, L. Liu, F. Zhang, K. Tao, E. Pippel, K. Domen, *Nano Lett.* **2011**, *11*, 3649–3655; b) Y. Liao, W. Que, P. Zhong, J. Zhang, Y. He, *ACS Appl. Mater. Interfaces* **2011**, *3*, 2800–2804.

[14] a) L. Tan, W. C. Crone, *Acta Mater.* **2002**, *50*, 4449–4460; b) X. M. Zhang, K. F. Huo, L. S. Hu, Z. W. Wu, P. K. Chu, *J. Am. Ceram. Soc.* **2010**, *93*, 2771–2778; c) Y. Xin, J. Jiang, K. Huo, T. Hu, P. K. Chu, *ACS Nano* **2009**, *3*, 3228–3234.

Received: February 2, 2012
Published online on February 29, 2012

CHEMPLUSCHEM

Supporting Information

Heterostructured TiO_2 Nanoparticles/Nanotube Arrays: In Situ Formation from Amorphous TiO_2 Nanotube Arrays in Water and Enhanced Photocatalytic Activity

Kaifu Huo,*[a, b] Hairong Wang,[b] Xuming Zhang,[a] Yue Cao,[b] and Paul K. Chu*[a]

cplu_201200024_sm_miscellaneous_information.pdf

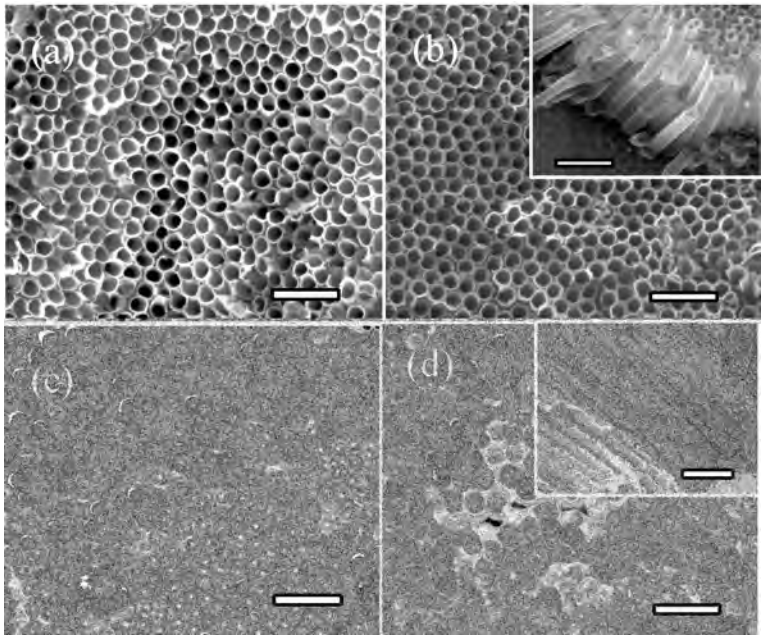

Figure S1 FE-SEM images of as-anodized TiO_2 NTAs after hydrothermal treatment at 200 °C for (a) 35 min, (b) 40 min, (c) 42 min, and (d) 45 min. The scale bar is 500 nm.

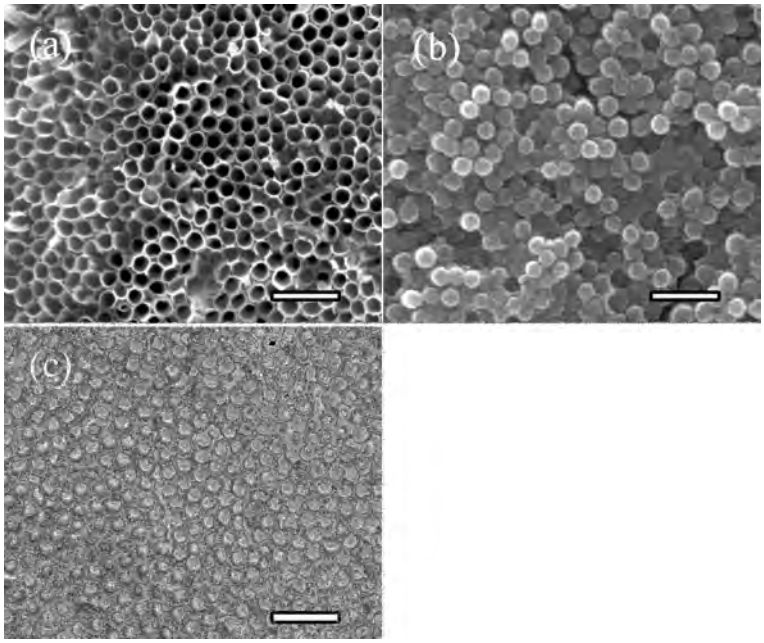

Figure S2 FE-SEM images of as-anodized TiO_2 NTAs after hydrothermal treatment in water at 100 °C for (a) 1 h and (b) 1.5 h as well as (c) at 80 °C for 8 h. The bar scale is 500 nm.

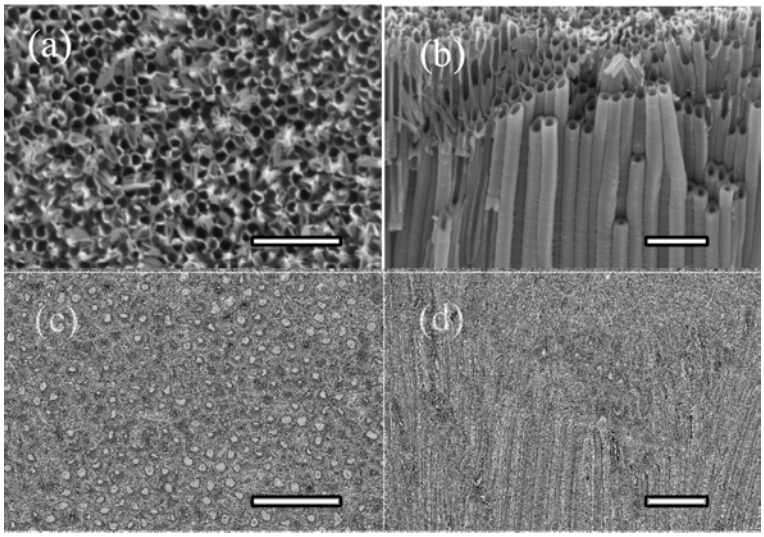

Figure S3 FE-SEM images of as-anodized TiO_2 NTAs after hydrothermal treatment in water in nitrogen circumstance. (a) and (b) at 90 °C for 5 h and (c) and (d) at 200 °C for 1 h. The bar scale is 500 nm. Nitrogen is bubbled into the water for 1 h and the autoclave is kept under nitrogen before sealing.

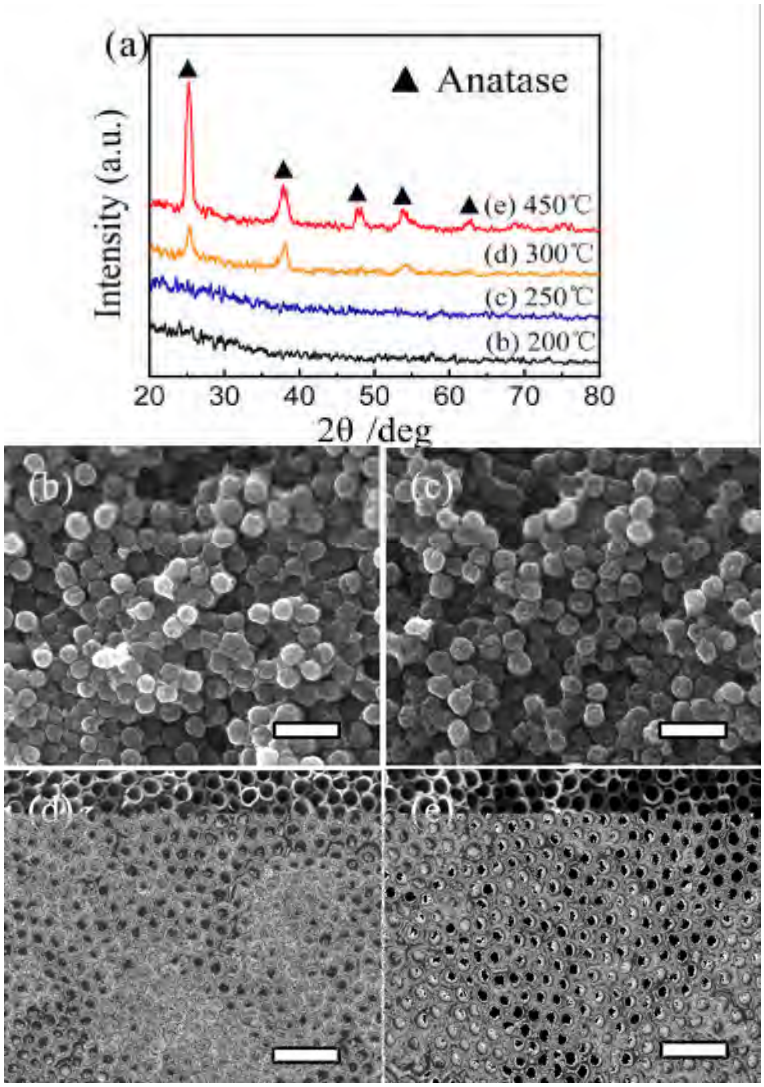

Figure S4. (a) XRD patterns of as-anodized TiO_2 NTAs sintered at 200 - 450 °C for 3 h in air together with the corresponding FE-SEM images of the pre-thermally treated specimens after undergoing hydrothermal treatment in water at 200 °C for 50 min (b) and (c), 20h (d) and (e). The scale bar is 500 nm.

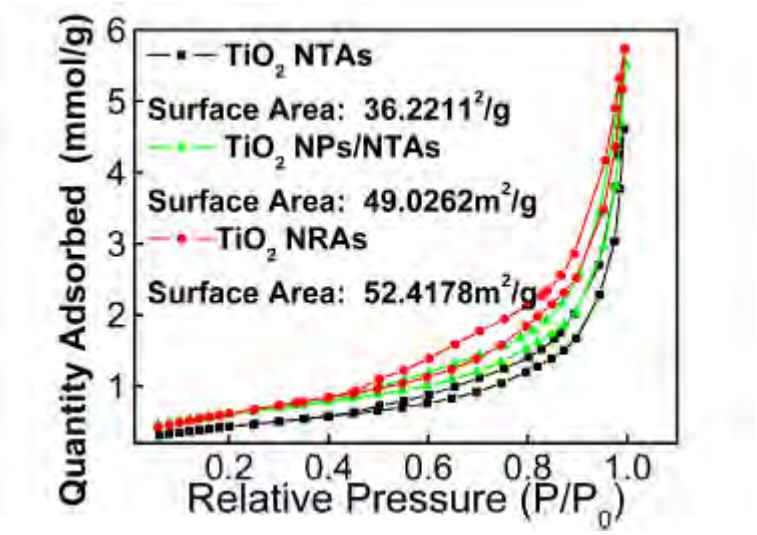

Figure S5 N_2 absorption/desorption isotherms of the thermally annealed TiO_2 NTs, TiO_2 NPs/NTAs and TiO_2 NRAs.